Acta Cryst. (1999). B**55**, 698–711

Long-range Coulomb forces and localized bonds

Christoph Preiser,[a] Jens Lösel,[b] I. David Brown,[c]* Martin Kunz[d] and Aniceta Skowron[e]

[a]*Institut für Anorganische Chemie, Johann Wolfgang Goethe-Universität, Frankfurt/Main, Germany,* [b]*Pfizer Central Research, Sandwich, Kent CT13 9NJ, England,* [c]*Institute for Materials Research, McMaster University, Hamilton, Ontario, Canada L8S 4M1,* [d]*Laboratory of Crystallography, ETH Zentrum, CH-8092 Zürich, Switzerland, and* [e]*Department of Materials Science and Engineering, McMaster University, Hamilton, Ontario, Canada L8S 4M1. E-mail: idbrown@mcmaster.ca*

(*Received 14 December 1998; accepted 9 March 1999*)

Abstract

The ionic model is shown to be applicable to all compounds in which the atoms carry a net charge and their electron density is spherically symmetric regardless of the covalent character of the bonding. By examining the electric field generated by an array of point charges placed at the positions of the ions in over 40 inorganic compounds, we show that the Coulomb field naturally partitions itself into localized regions (bonds) which are characterized by the electric flux that links neighbouring ions of opposite charge. This flux is identified with the bond valence, and Gauss' law with the valence-sum rule, providing a secure theoretical foundation for the bond-valence model. The localization of the Coulomb field provides an unambiguous definition of coordination number and our calculations show that, in addition to the expected primary coordination sphere, there are a number of weak bonds between cations and the anions in the second coordination sphere. Long-range Coulomb interactions are transmitted through the crystal by the application of Gauss' law at each of the intermediate atoms. Bond fluxes have also been calculated for compounds containing ions with non-spherical electron densities (*e.g.* cations with stereoactive lone electron pairs). In these cases the point-charge model continues to describe the distant field, but multipoles must be added to the point charges to give the correct local field.

1. Introduction

It is an assumption of all bond models of chemistry, models which have been widely and successfully used for well over a century, that one can gain a good description of the properties of a compound by ignoring all but the nearest-neighbour bonding interactions. Yet, calculations of inorganic structures based on realistic interatomic potentials show that the electrostatic interactions between second, third and even further neighbours are important and cannot be ignored. The apparent incompatibility between these two viewpoints has been one of the reasons why chemical-bond models have been sometimes viewed with suspicion. It is the purpose of this paper to show that the two approaches are not incompatible, since the Coulomb field responsible for the long-range forces naturally partitions itself into localized regions which link neighbouring atoms and which obey the same rules as those found empirically for chemical bonds. An examination of the behaviour of these links shows that long-range interactions are mediated through the application of Gauss' law around the intervening atoms. The electrostatic field thus provides a sound physical basis for the concept of the chemical bond and allows many of its properties to be rigorously derived.

In §2 we show that the only term that contributes to the long-range forces is the electric field produced by the net charges on the atoms (the Madelung field). In §3 we show that this field partitions itself into regions that link neighbouring atoms and we derive a number of laws that are obeyed by the electric flux which threads these regions. We then describe in §4 the empirical rules obeyed by bond valences in inorganic solids and show, in §5, that they are the same as those obeyed by the electric flux. Details of the calculation of the electrostatic flux are described in §6, while §7 compares the flux and bond valences for a variety of strained and unstrained structures. Our conclusions are summarized in §8.

2. Crystal energy and the Coulomb field

The energy of an inorganic solid consists of two terms, a classical electrostatic energy determined by the distribution of electric charge and a quantum mechanical term that prevents individual atoms from collapsing into each other (1)

$$W = W_{\text{electrostatic}} + W_{\text{qm}}. \qquad (1)$$

The quantum mechanical term W_{qm} is a short-range interaction which not only describes the Fermi repulsion between overlapping electron cores but, because it depends on the details of the electron density distribution, includes the influence of covalent bonding. In the ionic model it is usually represented by a short-range empirical potential. The electrostatic energy $W_{\text{electrostatic}}$

ISSN 0108-7681

can, in principle, be derived from the electrostatic field **E**, which is equal to the sum of the electrostatic fields of the individual atoms $\mathbf{E}_{\mathbf{atom}}$. $\mathbf{E}_{\mathbf{atom}}$ can in turn be represented by the sum of the three terms shown in (2).

$$\mathbf{E}_{\mathbf{atom}} = \mathbf{E}_{\mathbf{mono}} + \mathbf{E}_{\mathbf{mult}} + \mathbf{E}_{\mathbf{local}}. \quad (2)$$

In this equation $\mathbf{E}_{\mathbf{mono}}$ is the field generated by the point charge Q, which represents the net charge residing on the atom and which is assumed to be situated at the centre of the atom. $\mathbf{E}_{\mathbf{mono}}$ is given by (3).

$$\mathbf{E}_{\mathbf{mono}} = Q/(4\pi\varepsilon_0 r^2), \quad (3)$$

where r is the distance from the atom centre and, in this discussion, Q is measured in units of electron charge and the units are chosen so that ε_0 is 1.0. If the electron density of the atom is spherically symmetrical, $\mathbf{E}_{\mathbf{mono}}$ gives a fully correct description of the field generated by the atom in the region outside the atom itself, *i.e.* in the region where the electron density of the atom has fallen to zero. This is the term that is responsible for the long-range effects and is the term that will be examined in this paper.

If the electron density is not spherically symmetrical, the field outside the atom can again be correctly reproduced by adding as many point multipole terms as necessary to the original point charge Q. These constitute the term $\mathbf{E}_{\mathbf{mult}}$, which can be exactly calculated if the sizes and orientations of the multipoles are known. In most cases the multipoles are small relative to Q and in any case their field drops off rapidly with distance. Even if they make a significant contribution to the field in the immediate neighbourhood of the atom, their contribution at distances of more than a few ångströms from the centre of the atom is negligible (Bouhmaida *et al.*, 1997).

$\mathbf{E}_{\mathbf{mono}}$ and $\mathbf{E}_{\mathbf{mult}}$ thus give the exact electric field outside the atom regardless of the electron configuration within the atom. To obtain the correct field inside the atom requires the addition of the term $\mathbf{E}_{\mathbf{local}}$, which can be calculated if the electron density distribution is known, but for the present it is sufficient to note that $\mathbf{E}_{\mathbf{local}}$ is, by definition, zero outside the atom.

The total electric field in the crystal is obtained by adding the contributions from all the individual atoms in the crystal. At any particular point it will have contributions from $\mathbf{E}_{\mathbf{mono}}$ of all the atoms in the crystal, but only the immediately neighbouring atoms will contribute $\mathbf{E}_{\mathbf{mult}}$ and $\mathbf{E}_{\mathbf{local}}$ terms. The energy associated with these latter two terms can therefore be combined with W_{qm} into a short-range term, leaving only $\mathbf{E}_{\mathbf{mono}}$ to contribute to the long-range effects. The total energy can thus be rewritten as

$$W = W_{\mathrm{Madelung}} + W_{\mathrm{short\,range}}, \quad (4)$$

where W_{Madelung} is the Madelung energy derived from $\mathbf{E}_{\mathbf{mono}}$ and $W_{\mathrm{short\ range}}$ includes the effects of $\mathbf{E}_{\mathbf{local}}$ and $\mathbf{E}_{\mathbf{mult}}$, as well as W_{qm}. In the classical interatomic potential models that have recently proved so successful (Catlow, 1997), $W_{\mathrm{short\ range}}$ is represented by one of a number of short-range analytical functions with parameters which are fitted to the properties of the system. Since all the long-range interactions are included in the Madelung term W_{Madelung}, they are correctly represented by the field $\mathbf{E}_{\mathbf{Madelung}} = \sum\mathbf{E}_{\mathbf{mono}}$, which depends only on the magnitudes and positions of the monopole charges, Q.

The positions of the charges are assumed to be the same as the experimentally observed positions of atoms, but it is not so easy to see what the magnitudes of Q should be because the charge on an atom depends on how one defines an atom in the crystal. Various schemes have been proposed for calculating atomic charge, for example, Mullikan overlap populations or a space partitioning (Bader, 1990). In the present work the most appropriate definition of an atom is one that best meets the following criteria:

(1) each atom must carry a net charge equal to (or proportional to) the atomic valence (oxidation number);

(2) all the electron density in the crystal must be assigned to at least one atom (but may be divided between two or more atoms),

(3) subject to 1 and 2 above, the atoms have an electron density which is as close to being spherically symmetrical as possible in order to minimize $\mathbf{E}_{\mathbf{mult}}$.

It is not necessary at this point to choose any particular definition of an atom, only to know that it is possible to find a definition that meets these criteria. For example, the atoms might be treated as spheres. In this case the radius of the sphere would be chosen to ensure that criterion 1 is met. Cations would then have small radii and anions large radii. There would be considerable overlap between atoms, but if all the atoms carry their full charge, they must necessarily account for all the electron density in the crystal, thus satisfying criterion 2. The partitioning of electrons between atoms in regions of overlap would be performed in such a way as to best meet criterion 3. Any deviations from spherically symmetric atoms would be accommodated by the addition of point multipoles, but in most cases these multipoles are likely be small and of high order, particularly on the cation.

A justification for believing that such a definition is possible comes from the success of the two-body potential models in predicting both the structures and properties of inorganic crystals. In these models the atomic charge is routinely assumed to be equal to the formal oxidation state (Catlow, 1997). If such an assumption had no physical basis, the model clearly would not work.

3. The Madelung field of a crystal, $\mathbf{E}_{\mathbf{Madelung}}$

Consider the electrostatic field, $\mathbf{E}_{\mathbf{Madelung}}$, created by an infinite array of positive and negative point charges

placed at the positions of each of the atoms in a crystal. As has been pointed out by Bragg (1930), the lines that represent the electric field will not extend far in space, because at an energy minimum the lines of field will be as short as possible. Looked at from another point of view, the lines of field must remain short since their paths are not allowed to cross. All the lines of field starting at a positive charge will therefore terminate on the nearby negative charges and *vice versa*. The collection of all lines joining two given charges defines a region in space that represents the electrostatic link between them and, since every point in space will lie on a line of field, every point must belong to one or other of these link regions. Further, the boundaries between the link regions are necessarily zero-flux boundaries. Thus, $\mathbf{E}_{\mathbf{Madelung}}$ directly partitions space into a collection of localized link regions separated by zero-flux boundaries, as shown by the heavy lines in Fig. 1 for the (110) section of TiO_2 (rutile) which contains the Ti^{4+} and O^{2-} ions.

These link regions are characterized by the electrostatic flux Φ_{ij} connecting the two atoms i and j, given by (5)

$$\Phi_{ij} = \int \mathbf{E}_{\mathbf{Madelung}}.\mathrm{d}\mathbf{A}, \tag{5}$$

where the integration is taken over any cross-sectional area of the link region. These fluxes must obey Gauss' law (6) around each atom

$$\sum_j \Phi_{ij} = \oint \mathbf{E}_{\mathbf{Madelung}}.\mathrm{d}\mathbf{A} = Q_i, \tag{6}$$

where the sum is taken over all links connected to Q_i and the integration is taken over any closed surface surrounding Q_i.

The law of conservation of energy can be applied to this system if the potential differences between the atoms can be calculated. To do this it is convenient to treat each link as a capacitor C_{ij} supporting a potential difference P_{ij}. The electric flux Φ_{ij} which threads this capacitor must equal the charge q_{ij} on the capacitor 'plates', q_{ij} being those portions of the atomic charges of i and j that contribute to Φ_{ij}. Since each charge Q_i will contribute to a number of such links, the sum of all the link charges q_{ij} will just be the total charge Q_i

$$Q_i = \sum_j q_{ij}. \tag{7}$$

The potential P_{ij} across the capacitor is given by the capacitor equation

$$P_{ij} = q_{ij}/C_{ij}. \tag{8}$$

Since q_{ij} is equal to the flux Φ_{ij}, (8) can also be written as

$$P_{ij} = \Phi_{ij}/C_{ij}. \tag{9}$$

The law of conservation of energy requires that the sum of the potentials P_{ij} around any closed loop be zero, hence

$$0 = \sum_{\text{loop}} P_{ij} = \sum_{\text{loop}} \Phi_{ij}/C_{ij}, \tag{10}$$

where each loop will contain a number of links and the flux of each is taken as positive or negative, according to the direction in which it is traversed. Equations (6) and (10) constitute the Kirchhoff equations for a system of capacitors.

Since the electric potential is singular at a point charge, the potential difference between a point positive and a point negative charge will be infinite and C_{ij} will be zero. This singularity can be avoided by replacing each point charge by a closed equipotential shell and distributing the charge Q_i over this surface in such a way as to leave the external field unchanged. The link regions are now bounded at their ends by that portion of the charged equipotential surface on which their field lines start or terminate. These surfaces therefore act as the plates of the capacitor carrying the charge q_{ij}. For this arrangement C_{ij} and P_{ij} are finite and, in principle, calculable.

The values of C_{ij}, of course, depend on which equipotential surface is used to represent the atom. Since these surfaces can be arbitrarily chosen, it might be supposed that all the values of C_{ij} could be arbitrarily set to the same value so that they cancel in (10). However, the number of charges for which the equipotential surface can be arbitrarily chosen is always less than the number of links between them. If there are N charges in the array, the equipotential surfaces can only be chosen in such a way that the $N-1$ links in the spanning tree are assigned arbitrary values of C_{ij}. For the remaining links, *i.e.* the links that close the loops in the network, a knowledge of only the topology is not sufficient to determine C_{ij}. To find these, the geometry of the array, *i.e.* the positions of the charges, must also be known.

As mentioned above, the portion of the equipotential surface on which the flux lines start or end must, according to Gauss' theorem, carry a charge equal to q_{ij}.

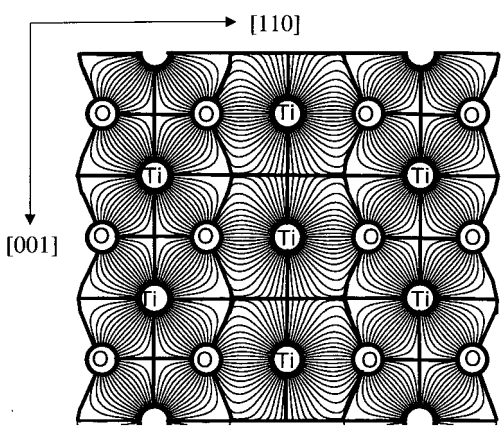

Fig. 1. A representation of the Madelung field of rutile (TiO_2) in the $(1\bar{1}0)$ plane $(x,1-x,z)$. The light lines represent the field lines, the heavy lines show the zero-flux boundary that partitions space into link (bond) regions.

To find Φ_{ij}, therefore, it is only necessary to determine q_{ij}. This can easily be performed if the charge is uniformly distributed over the surface, which will be the case if the surface is shrunk to a small sphere around the position of the point charge, since here the field is essentially spherically symmetric. In this case q_{ij} is given by

$$q_{ij} = Q_i A_{ij}/(4\pi r_i^2) = Q_j A_{ji}/(4\pi r_j^2), \qquad (11)$$

where r_i and r_j are the radii of the equipotential spheres and A_{ij} is the surface area of that part of the equipotential sphere around i that forms the end boundary of the link region between atoms i and j. The flux can then be found from the areas A calculated by determining the boundaries of the link regions on the equipotential surface, as described in detail in the *Appendix*.

Fig. 1 shows an exact representation of the Madelung field from an array of point charges placed at the positions of the atoms in rutile, TiO_2. The boundaries of the link regions are shown with a heavy line. Such a localization of the field is not incompatible with the long-range nature of the electrostatic force. The mechanism for the long-range interaction is through the application of Gauss' law around each atom. As shown in Fig. 2, the removal of an O^{2-} ion from the perfect lattice shown in Fig. 1 results in a redistribution of the flux. The flux that originally terminated on the missing anion now terminates on anions in the second neighbour shell but, in order to accommodate this new flux, the anions of the second neighbour shell must shed flux to the fourth neighbour shell and so on. A ripple of flux relaxation spreads out from any change made in the lattice, the long-range effects being mediated through a redistribution of the flux around the intervening atoms in accordance with Gauss' theorem. Thus, long-range interactions are achieved by an inductive effect and are quite compatible with the partitioning of the field into the localized link regions.

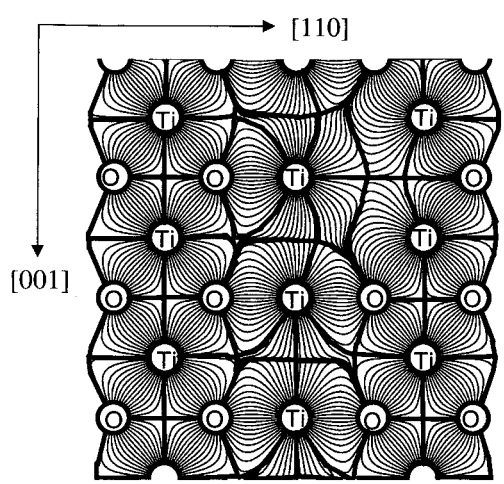

Fig. 2. A representation of the Madelung field of rutile in the $(1\bar{1}0)$ plane with one O^{2-} ion removed. The conventions are the same as in Fig. 1.

The distribution of flux between the links is completely determined by the two electrostatic Kirchhoff equations (6) and (10), provided that the topology of the link regions is known, *i.e.* it is known which charges are linked. Unfortunately, as pointed out above, the values of C_{ij} in (10) cannot be determined *a priori*, since they depend on the geometry adopted by the array. The factors which determine this geometry, and hence C_{ij}, in equilibrium structures are discussed in §5.

4. The bond-valence model

Before proceeding further it is useful to review the properties of chemical bonds in inorganic compounds as they have been determined empirically through a study of known inorganic structures. The similarity between these empirical rules and the properties of $\mathbf{E}_{\mathbf{Madelung}}$ should be readily apparent.

Pauling (1929) was one of the first in recent times to apply the concept of a chemical bond to inorganic solids. The tendency of cations to surround themselves with anions in a way that provides local charge neutrality was the basis of his electrostatic valence principle that describes the behaviour of these bonds. Shortly after, Bragg (1930) pointed out that this principle has a graphic representation in the lines of electrostatic field, but the implications of this observation were not further explored. In recent years the electrostatic-valence principle has been elaborated into the bond-valence model, an empirical theory that allows a quantitative prediction of the geometry of many inorganic compounds (Brown, 1992*a*). The theory treats a compound as an infinite network of atoms linked by bonds. For crystals, this can be reduced to a finite network comprising a single formula unit such as the network of TiO_2, whose graph is shown in Fig. 3. Each line represents a different bond, so that Ti^{4+} is six-coordinated and O^{2-} is three-coordinated. The bond-valence model itself is restricted to compounds whose bond graph contains two types of atoms, labelled cations and anions according to the sign of their valence, with a further formal restriction that bonds may only link ions of opposite sign.

Each atom i in the graph is assigned a formal charge equal to its *atomic valence* or oxidation state (V_i) and each bond between atoms i and j is assigned a *bond valence* (s_{ij}). The bond valence is determined by

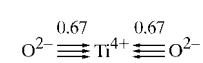

Fig. 3. The bond graph of rutile (TiO_2). The valences of the atoms and theoretical valences of the bonds are shown.

assuming that the valence of an atom is distributed as uniformly as possible among the bonds that it forms, a condition that is formally expressed by two *network equations*. The first, known as the *valence-sum rule* (12), states that the sum of the valences of all the bonds meeting at an atom i is equal to the valence of the atom

$$\sum_j s_{ij} = V_i. \quad (12)$$

The second equation is the condition that requires the valence to be distributed as uniformly as possible among the bonds in a way that is consistent with (12). It is known as the *equal valence rule* and is formally achieved (Brown, 1992*b*) by ensuring that the sum of all directed bond valences around a closed loop is zero, as expressed by

$$\sum_{\text{loop}} s_{ij} = 0. \quad (13)$$

These two equations can be used to predict a unique bond valence s_{ij} (referred to here as the *theoretical bond valence*) for every bond in the graph, as shown in Fig. 3.

Theoretical bond valences s_{ij} are often found empirically to be very close to *experimental bond valences* S_{ij} calculated from the observed bond lengths R_{ij} using

$$S_{ij} = \exp[(R_o - R_{ij})/B]. \quad (14)$$

Here R_o and B are empirical parameters whose values for different bonds have been tabulated by Brown & Altermatt (1985) and Brese & O'Keeffe (1991).

In many crystals the experimental and theoretical bond valences are found to agree within the limits of experimental accuracy, but there are a number of structures in which they differ significantly. The discrepancy between these values is given for a number of typical compounds by σ_3 in Table 1. On examination, structures with large σ_3 are all found to be subject to additional constraints which cause the bonds to be strained (Brown, 1992*a*). The most common constraints are electronic anisotropies (*e.g.* Jahn–Teller distortions around transition metals and stereoactive lone pairs around main-group elements in lower oxidation states), cation–cation or anion–anion repulsion (*e.g.* in hydrogen bonds; Brown, 1995) and lattice incommensurations (*e.g.* in perovskite layer compounds). Although the experimental bond valences in these compounds do not obey the equal valence rule (13), most continue to obey the valence-sum rule (12). In this paper a structure is assumed to be strained if the root-mean-square deviation between the experimental and theoretical bond valences, $\sigma_3 = \langle(S_{ij} - s_{ij})^2\rangle^{1/2}$, is greater than 0.05 valence units (v.u.).

Table 1. *Agreement between the bond flux and bond valences for compounds used in this study*

ICSD = Collection code in the Inorganic Crystal Structure Database; $\sigma_1 = \langle(\Phi_{ij} - s_{ij})^2\rangle^{1/2}$; $\sigma_2 = \langle(\Phi_{ij} - S_{ij})^2\rangle^{1/2}$; $\sigma_3 = \langle(S_{ij} - s_{ij})^2\rangle^{1/2}\Phi$ = bond flux; s = theoretical bond valence; S = experimental bond valence; N = number of bonds around the electronically distorted cation included in the network used for calculating s_{ij}; $R_1 = \langle(V_i - \sum_j S_{ij})^2\rangle^{1/2}$.

ICSD	Compound	σ_1	σ_2	σ_3	R_1
Unstrained structures					
100676	$CaCO_3$ Calcite	0.07	0.08	0.02	
38233	Cu_2O	0.04	0.06	0.02	
67453	ZnS Wurtzite†	0.02	0.06	0.05	
10286	$CaCrF_5$†	0.02	0.03	0.03	
31321	TiO_2 Rutile†	0.03	0.05	0.03	
60378	ZnS Sphalerite†	0.00	0.04	0.04	
15198	$CaCO_3$ Aragonite	0.06	0.04	0.04	
9852	TiO_2 Anatase	0.05	0.03	0.04	
200405	$NaClO_4$†	0.10	0.06	0.05	
63364	$CsClO_4$	0.05	0.03	0.05	
34243	Ga_2O_3	0.05	0.05	0.05	
16382	$CaSO_4$	0.08	0.06	0.05	
9672	$MgCaSi_2O_6$	0.06	0.04	0.05	
Sterically strained: hydrogen bonds					
34401	$Mg(OH)_2$	0.18	0.02	0.21	
1914	$Li(H_2O)_3ClO_4$	0.11	0.07	0.0	
34447	KH_2PO_4	0.13	0.05	0.14	
Sterically strained: cation–cation repulsion					
201096	Fe_2O_3	0.09	0.03	0.11	
1462	Ti_2O_3	0.07	0.04	0.03	
Sterically strained: lattice incommensuration					
75263	$LiGaSi_2O_6$	0.07	0.05	0.07	0.09
31005	$Mg_3(PO_4)_2$	0.08	0.08	0.06	0.10
39159	$SrZnGe_2O_7$	0.06	0.06	0.07	0.17
69387	$CaZnGe_2O_7$	0.06	0.09	0.10	0.29‡
68381	La_2CuO_4	0.08	0.10	0.17	0.27‡

ICSD	Compound	σ_1	σ_2	σ_3	N
Electronically strained: lone pair					
16220	Tl_2O	0.01	0.02	0.02	3
2114	As_2O_3 cubic	0.21	0.22	0.01	3
4108	As_2O_3 monoclinic	0.23	0.23	0.04	3
1944	Sb_2O_3 cubic	0.27	0.26	0.01	3
		0.23	0.23	0.46	6
2033	Sb_2O_3 monoclinic	0.35	0.26	0.10	3
		0.14	0.24	0.34	5
2374	Bi_2O_3 alpha	0.44	0.22	0.26	3
		0.10	0.19	0.25	5, 6
72366	SeO_2	0.59	0.42	0.20	3
		0.27	0.33	0.56	6
62898	TeO_2 alpha	0.25	0.33	0.31	4
		0.24	0.29	0.49	6
78387	I_2O_5	0.77	0.55	0.28	3
		0.26	0.46	0.63	5
9869	TeF_4	0.25	0.28	0.13	5
		0.18	0.27	0.35	7
26056	$TeCl_4$	0.11	0.21	0.12	6
79	TeI_4	0.13	0.16	0.09	6
Electronically strained: transition metals					
36408	TiO_2 Brookite	0.08	0.06	0.11	6
60767	V_2O_5	0.25	0.19	0.13	5
		0.31	0.22	0.52	6
21064	CaV_2O_6	0.26	0.11	0.32	6

5. Coulomb field and chemical bonds

The parallels between the electrostatic field model and the bond-valence model should be apparent. The frag-

Table 1 (*cont.*)

ICSD	Compound	σ_1	σ_2	σ_3	N
2899	$LiVO_3$†	0.15	0.10	0.15	4
		0.25	0.11	0.36	6
16031	CrO_3†	0.54	0.41	0.17	4
		0.34	0.44	0.73	6
60821	Mn_2O_7	0.34	0.30	0.12	4

† Full details of these compounds are given in Table 2. Full details of the remaining compounds are given in Table S2 which has been deposited (see footnote on p. 704). ‡ The archetype structures used in the calculation are unstable. The true structures have lower symmetry.

mentation of the electrostatic field into link regions suggests that the link regions can be identified with chemical bonds. The similarity between the Kirchhoff equations (6) and (10) and the network equations (12) and (13) suggests that, since the point charges Q_i have been set equal to the atomic valences V_i, the flux Φ_{ij} threading a link region can be identified with the bond valence s_{ij}. We propose the following hypothesis:

Given that the atomic valence V_i is equal to the formal charge Q_i, the fluxes linking atoms in the electrostatic model are the same as the bond valences assigned using the bond-valence model.

If this hypothesis is correct, the flux in the Coulomb field provides a rigorous physical definition of bond valence, a quantity which has hitherto been only empirically defined, either in terms of bond length (experimental bond valence) or in terms of bond topology (theoretical bond valence). With this new definition, Gauss' theorem corresponds to the valence-sum rule (12), which must then be rigorously true, and an atom's coordination number is precisely defined as the number of neighbouring atoms which are linked to it by electrostatic flux.

Even though the valence-sum rule (12) can be identified with Gauss' theorem, it is not possible to derive the equal-valence rule (13) directly from the energy conservation equation (10) since the quantity C_{ij} appears in (10), but no equivalent term appears in (13). These two equations can only be equivalent if the values of C_{ij} cancel in (10). As discussed in §3, the values of C_{ij} depend on the geometry of the array of charges, that is, on the positions occupied by the atoms in three-dimensional space and can thus only be calculated if the geometry of the structure is known. Further, (13) does not hold for all observed structures, only for those in which there are no additional constraints causing the bonds to be strained, *i.e.* for those structures with $\sigma_3 \leq 0.05$ v.u. Therefore, it is only for the unstrained structures, those where (13) is obeyed, that the values of C_{ij} are expected to cancel. The simplest way to test the equivalence of (13) and (10) is to compare the fluxes Φ_{ij} calculated for the array of point charges in unstrained structures, with the theoretical bond valences s_{ij} calculated using the network equations. In §7 it is shown that these are the same within the limits of experimental uncertainty.

Although a rigorous proof that (13) and (10) are identical in unstrained structures is not possible, their equivalence can be shown to be plausible. To understand the origin of the equal-valence rule, it is necessary to consider the repulsive forces that keep the atoms apart. These forces are short range, dropping to negligible values at separations of two or three ångstroms, but becoming very large as the atoms are forced close together. Originally the repulsive potential was modelled using an inverse power law potential (Born & Landé, 1918), but later an exponential potential (15) was shown to be closer to the correct physical form (Born & Mayer, 1932)

$$W_{\text{short range}} = A.\exp(-R_{ij}/\rho), \tag{15}$$

where A and ρ are fitted constants.

In order to minimize the Madelung energy the atoms should be brought as close together as possible, but at short distances shortening a bond increases the repulsive energy by more than the electrostatic energy is reduced, so for a given bond flux the length of a bond is determined primarily by the repulsive energy. For an atom surrounded by chemically identical ligands, the minimum in the total energy will occur when the ligands are all at the same distance. Under these conditions the bonds will tend to have identical capacitances as required if (13) and (10) are to be identical. Although this is only a qualitative argument, it leads one to expect that the equal-valence rule (13) will be obeyed in unstrained structures and it suggests that the correlation between flux and bond length will have an exponential form. The similarity between the forms of (14) and (15) is therefore no coincidence.

It should be pointed out that neither the electrostatic nor the bond-valence model describes homopolar bonding, that is the bonding that occurs between two anions or between two cations. A formal statement of this constraint is that the graph of the bond network must be bipartite, containing two different kinds of nodes, cations and anions, with bonds allowed only between nodes of opposite sign. One consequence is that only even-membered rings (loops) are allowed in the bond networks discussed in this paper.

6. Calculation of the Coulomb field

We have calculated the Madelung field $\mathbf{E}_{\mathbf{Madelung}}$ and the bond fluxes Φ_{ij} for over 40 observed crystal structures as described in the *Appendix*. The structural information has been taken from the Inorganic Crystal Structure Database (ICSD; Bergerhoff *et al.*, 1983) and the compounds used in this study are listed in Table 1 together with their ICSD collection code and various

figures of merit. σ_1 is the root-mean-square difference between the electrostatic flux Φ_{ij} and the theoretical bond valence s_{ij}. σ_2 is the root-mean-square difference between Φ_{ij} and the experimental bond valence S_{ij}. σ_3 is the root-mean-square difference between the theoretical and experimental bond valences and is used to determine which structures are unstrained. For structures showing lattice-induced strain we also give the global instability index R_1, which is the root-mean-square difference between the experimental bond-valence sums and the atomic valences. R_1 measures the extent to which the valence-sum rule is violated, hence the extent of the lattice-induced strain (Salinas-Sanchez *et al.*, 1992), with crystals in which R_1 exceeds 0.2 v.u. generally being unstable. Table 2 lists the electrostatic fluxes Φ_{ij} and the theoretical s_{ij} and experimental S_{ij} bond valences for a selection of typical structures. The corresponding values for the remaining structures are given in Table S2.†

7. Discussion

7.1. *Unstrained structures*

It is convenient to discuss the results according to the type of strain present. In this subsection the unstrained structures are discussed. Subsequent subsections discuss structures with strains that result from steric effects (§7.2) and structures with electronic anisotropies, divided into those with cations containing stereoactive lone pairs (§7.3.1) and those containing transition metal cations (§7.3.2).

The strains discussed in this paper are all measured with reference to the theoretical bond lengths determined using the network equations (12) and (13) together with (14). Unstrained structures are therefore defined as those in which the root-mean-square difference between the theoretical bond valences (s_{ij}) and the experimental bond valences (S_{ij}) does not exceed 0.05 v.u. (σ_3 in Table 1) and in which there are no angular distortions of the kind found around cations with stereoactive lone pairs. It is worth pointing out that an unstrained structure is not necessarily one with regular coordination. Coordination spheres in which all the bonds are equal may be strained and, conversely, coordination spheres in which the bonds have different lengths may be unstrained. Crystals with the NaCl structure may be strained because the expected bond lengths cannot always be achieved without causing excessive cation–cation or anion–anion repulsion. $CaCrF_5$ (Table 2) is an example of an unstrained structure in which the bonds have different lengths because the anions are not all equivalent.

† Supplementary data for this paper are available from the IUCr electronic archives (Reference: SH0127). Services for accessing these data are described at the back of the journal.

Table 2. *Bond lengths, electrostatic fluxes and bond valences in selected structures*

R_{ij} = bond length, Φ_{ij} = flux, s_{ij} = theoretical bond valence calculated using the primary coordination sphere, s'_{ij} = theoretical bond valence calculated using the primary and secondary coordination spheres, S_{ij} = experimental bond valence.

	R_{ij}	Φ_{ij}	s_{ij}	s'_{ij}	S_{ij}
$CaCrF_5$ (ICSD 10286; Wu & Brown, 1973)					
Cr—F3 × 2	1.848	0.58	0.61		0.60
Cr—F2 × 2	1.918	0.47	0.48		0.49
Cr—F1 × 2	1.940	0.41	0.41		0.47
Ca—F3 × 2	2.215	0.39	0.39		0.36
Ca—F2 × 2	2.292	0.29	0.26		0.30
Ca—F2 × 2	2.390	0.23	0.26		0.23
Ca—F1	2.494	0.17	0.18		0.17
ZnS (sphalerite) (ICSD 60378; Jumpertz, 1955)					
Zn—S × 4	2.345	0.50	0.50		0.54
ZnS (wurtzite) (ICSD 67453; Kisi & Elcombe, 1989)					
Zn—S × 3	2.342	0.48	0.50		0.55
Zn—S	2.347	0.53	0.50		0.54
Zn—S	3.914	0.02	–		0.01
$NaClO_4$ (ICSD 200405; Wartchow & Berthold, 1978)					
Na—O1 × 2	2.386	0.23	0.12		0.21
Na—O2 × 2	2.518	0.13	0.12		0.14
Na—O1 × 2	2.644	0.08	0.12		0.10
Na—O2 × 2	2.707	0.07	0.12		0.09
Cl—O1 × 2	1.432	1.59	1.75		1.72
Cl—O2 × 2	1.437	1.61	1.75		1.69
Cl—O2 × 2	3.392	0.18	–		0.01
Cl—O1 × 2	3.863	0.04	–		0.00
Cl—O2 × 4	4.269	0.03	–		0.00
TiO_2 Rutile (ICSD 31321; Gonschorek, 1982)					
Ti—O × 4	1.948	0.64	0.67		0.70
Ti—O × 2	1.981	0.68	0.67		0.64
Ti—O × 4	3.487	0.03	–		0.01
CrO_3 (ICSD 16031; Stephens & Cruickshank, 1970)					
Cr—O3	1.576	1.16	2.00	1.00	1.80
Cr—O2	1.580	1.31	2.00	1.00	1.78
Cr—O1 × 2	1.748	0.96	1.00	1.00	1.13
Cr—O3	3.218	0.62	–	1.00	0.02
Cr—O2	3.341	0.34	–	1.00	0.02
Cr—O2 × 2	3.581	0.17	–	–	0.01
Cr—O3 × 2	3.913	0.09	–	–	0.00
Cr—O1 × 2	4.166	0.03	–	–	0.00
Cr—O3	4.264	0.02	–	–	0.00
Cr—O1 × 2	4.547	0.03	–	–	0.00
$LiVO_3$ (ICSD 2899; Shannon & Calvo, 1973)					
Li1—O2 × 2	1.997	0.20	0.20	0.08	0.24
Li1—O1 × 2	2.125	0.18	0.15	0.29	0.17
Li1—O1 × 2	2.339	0.12	0.15	0.29	0.09
Li2—O1 × 2	2.106	0.31	0.28	0.34	0.18
Li2—O3 × 2	2.166	0.14	−0.10	0.03	0.15
Li2—O2 × 2	2.670	0.05	0.32	0.18	0.04
V—O2	1.629	1.33	1.48	0.70	1.60
V—O1	1.662	1.32	1.42	1.07	1.46
V—O3	1.764	0.93	1.05	0.91	1.11
V—O3	1.848	0.85	1.05	0.91	0.89
V—O2	3.051	0.26	–	0.70	0.03
V—O2	3.247	0.12	–	0.70	0.02
V—O3	3.565	0.07	–	–	0.01
V—O2	3.625	0.05	–	–	0.01

Fig. 4 shows the correlation between the electrostatic fluxes Φ_{ij} and the experimental bond valences S_{ij}, for the unstrained structures listed in Table 1. The graph is similar if the fluxes are plotted against the theoretical bond valences since the experimental and theoretical valences are, by definition, very similar for these structures. The correlation is remarkably good, thus supporting the hypothesis that the bond valences and electrostatic fluxes are the same. Only for the strongest bonds are the fluxes a little smaller than the bond valences and this is a consequence of the appearance in the Madelung field of a number of very weak bonds between atoms that are not normally considered to be part of the coordination sphere. We refer to these as 'tertiary bonds', recognizing that the term 'secondary bond' has been used in a different sense to describe the weak bonding found around cations with stereoactive lone pairs (Alcock, 1972, see §7.3.1). Examples of tertiary bonds can be found in a number of the compounds listed in Table 2, particularly $NaClO_4$, and they appear in Fig. 4 on the vertical axis. The diversion of flux from the primary bonds into the tertiary bonds accounts for the small systematic differences shown in Fig. 4.

The idea that some of the longer cation–anion distances might contribute to weak, but significant, chemical bonding was proposed by Alig & Trömel (1992) using a definition of coordination number based on the Frank-Kasper construction. Their suggestion is confirmed by the present observation that atoms separated by as much as 3 or 4 Å can be linked by electrostatic flux, although there is not a one-to-one correlation between the bonds found using the Frank-Kasper construction and those defined by the Madelung field.

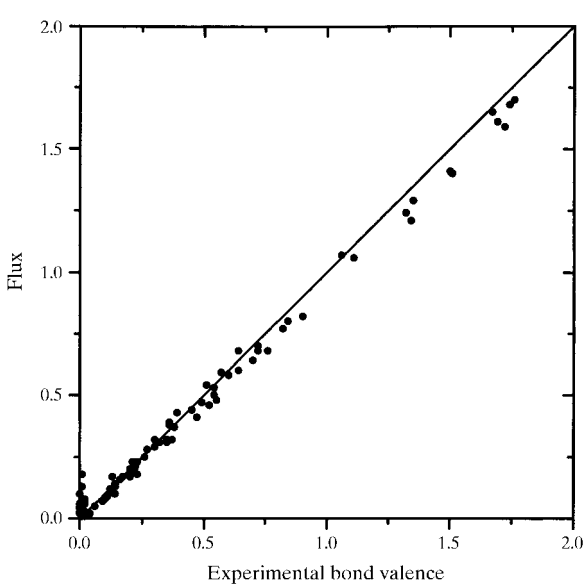

Fig. 4. Flux *versus* experimental bond valence for unstrained structures.

The relationship between primary and tertiary bonds can be seen in Fig. 5, which shows the regions subtended by different bonds on the equipotential sphere that surrounds the Ti^{4+} ion in rutile. The six primary bonds clearly occupy the major portion of the surface, the tertiary bonds being confined to a thin section close to the (001) mirror plane between the primary bonds. Fig. 6 shows the lines of field in this plane. The large blank section between the O atoms is a boundary between two bond regions that lie above and below the plane, hence, by symmetry, it is a plane devoid of field lines. Bordering this region are four tertiary bonds and, although they occupy a large amount of space in this section, examination of Fig. 5 shows that they do not extend very far perpendicular to this plane. They represent a small leakage of flux between the primary bonds to atoms whose proximity is an accident of the crystal geometry. Because the tertiary bonds are necessarily much longer than primary bonds, they all have lengths corresponding to very small experimental bond valences, generally less than 0.03 v.u.

In unstrained structures there is usually a clear distinction between the primary bonds, those normally included in the chemical description of a compound and the much longer tertiary bonds. The latter are typically longer than 3 Å and generally quite weak, with fluxes of less than 0.03 v.u. Primary and tertiary bonds are further distinguished by the fact that good agreement between the theoretical and experimental bond valences can only be obtained if the tertiary bonds are omitted from the network calculation, that is, the geometry of the primary coordination sphere is determined only by the topology of the primary bonds. The presence or absence of tertiary bonds has only a minor effect on the geometry. Tertiary bonds are only found where there are opportunities for flux to reach second-neighbour anions. This is well illustrated by the differences in the bonding

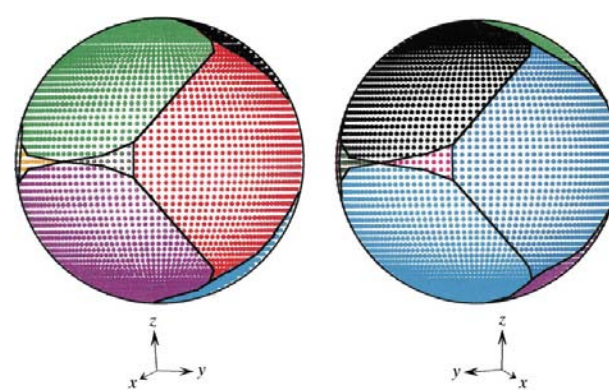

Fig. 5. A representation of opposite sides of an equipotential sphere around a Ti atom in rutile. Every point represents the starting point of a field line. Points representing field lines to different atoms are shown with a different colour. The lines show the boundaries of the bond regions on the equipotential sphere.

found in the sphalerite and wurtzite forms of ZnS (Table 2) illustrated in Fig. 7. The primary coordination in ZnS is determined by the properties of the Zn^{2+} and S^{2-} ions, namely Zn^{2+} is four-coordinate, so that in both structures Zn^{2+} is tetrahedrally surrounded by four S^{2-} neighbours at essentially the same distance. The differences between the structures arise from the different ways in which these tetrahedra are arranged. In the cubic sphalerite structure all the tetrahedral faces are shared with octahedral cavities, one of which is shown in Fig. 7(*a*), but in the trigonal wurtzite structure one face is shared with a vacant tetrahedral cavity which places an S^{2-} ion directly over the shared face (Fig. 7*b*), allowing flux to leak through this face to the S^{2-} ion in the second coordination sphere. The wurtzite form therefore contains one tertiary bond, while the sphalerite form contains none.

Tertiary bonds are found around many cations, but whether they will occur in any particular compound is determined by details of the crystal structure. The number of tertiary bonds tends to increase with the bonding strength of the cation, that is, more tertiary bonds are likely to be found around highly charged cations with low coordination number, such as Cl^{7+} in ClO_4^-. The diversion of flux from primary to tertiary bonds around these cations is responsible for the relatively low values of the fluxes found for the strongest bonds illustrated in Fig. 4.

One should be cautious in ascribing too much significance to the tertiary bonds. Their fluxes are small and could be significantly altered by changes in the model, such as including $\mathbf{E}_{\mathbf{mult}}$ or $\mathbf{E}_{\mathbf{local}}$ in the flux calculation or by changing the method by which the flux is calculated. More work is needed to clarify their role in crystal chemistry.

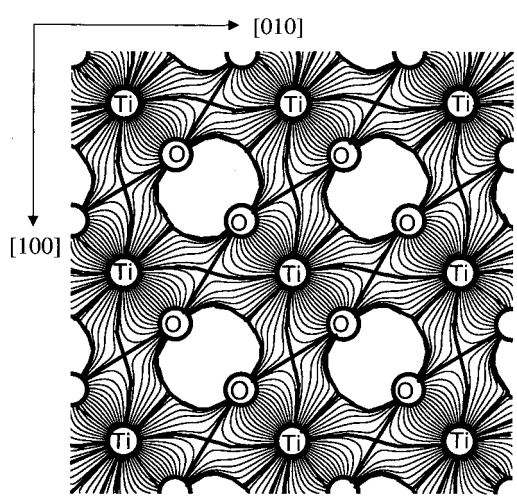

Fig. 6. A representation of the valence field of rutile (TiO_2) in the crystallographic (001) mirror plane at $z = 0$. The conventions are the same as in Fig. 1.

7.2. *Sterically strained structures*

Steric strains arise from a number of factors, such as non-bonded repulsions and lattice incommensurations, which are related to the way in which the atoms pack together in a crystal.

The asymmetry found in hydrogen bonds, for example, is a consequence of repulsion between the donor and acceptor anions which keeps the hydrogen bond long (Brown, 1995). Owing to this strain, which ensures that the H atom will bond unequally to its two (or more) neighbours, the theoretical bond valences are expected to differ considerably from the experimental valences (see σ_3 in Table 1). However, the agreement between the experimental valences and the fluxes, indicated by σ_2 in Table 1, is satisfactory, given the difficulties in determining the positions of the H atoms and the consequent difficulties in assigning good experimental valences. We have examined only three hydrogen-bonded crystals, recognizing that hydrogen bonds deserve a far more extensive treatment than we can give them in this paper. Apart from confirming that there is a reasonable agreement between the fluxes and the experimental bond valences, there are few surprises. In $Mg(OH)_2$, as expected, each H^+ ion forms three weak links (0.08 v.u.) to O^{2-} ions in the adjacent layer. The only new feature that appears in our calculations is the bifurcated hydrogen bond, shown in Fig. 8, that occurs with the double hydrogen bonds found in KH_2PO_4.

Two compounds with cation–cation repulsion (both with the corundum structure) have been examined. The

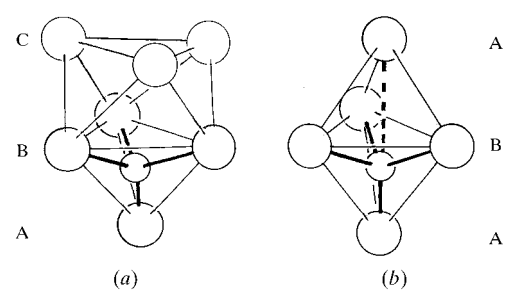

Fig. 7. The environment of Zn^{2+} in ZnS in (*a*) the sphalerite structure and (*b*) the wurtzite structure. The large circles represent S^{2-}, the small circles Zn^{2+}. The letters *A*, *B* and *C* refer to the stacking sequence of close-packed S^{2-} layers. The broken line represents the tertiary bond.

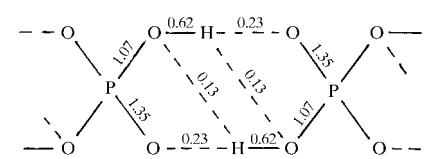

Fig. 8. Bond fluxes in KH_2PO_4 illustrating that the donor O atoms in the PO_4^{3-} ion also act as hydrogen bond acceptors.

cations in Fe_2O_3 and Ti_2O_3 lie at the centre of oxygen octahedra which are associated in pairs sharing a common face. The cations repel each other across this face, resulting in three long and three short cation–oxygen bonds. Since the network equations assign the same valence (0.5 v.u.) to all bonds, the agreement between the theoretical and experimental bond valences, σ_3, is poor. However, within experimental uncertainty, the experimental valences and the fluxes are the same ($\sigma_2 < 0.05$ v.u.)

A third type of steric strain is found in structures in which the crystallographic repeat can only be maintained if some of the bonds are stretched and others compressed, a condition frequently encountered in the perovskite-related structures. These strains are responsible for many unusual properties such as ferroelectricity and superconductivity (Brown, 1991). As a result of a strain in which the bonds around some atoms are stretched while the bonds around other atoms are compressed, the valence-sum rule is typically violated so that a good estimate of the degree of strain is given by the Global Instability Index R_1, which is the root-mean-square deviation of the experimental bond-valence sums from the atomic valences (Salinas-Sanchez *et al.*, 1992). If the strain is sufficiently large ($R_1 > 0.2$) the structure is unstable. Both $CaZnGe_2O_7$ and La_2CuO_4 (Table 1) exist as structures with lower symmetry than the archetype structures used in the present calculations. In spite of the failure of the valence-sum rule in many of these compounds, the good agreement between the flux and experimental bond valence (σ_2 in Table 1) suggests that observed structures still obey the equal-valence rule as far as the constraints allow.

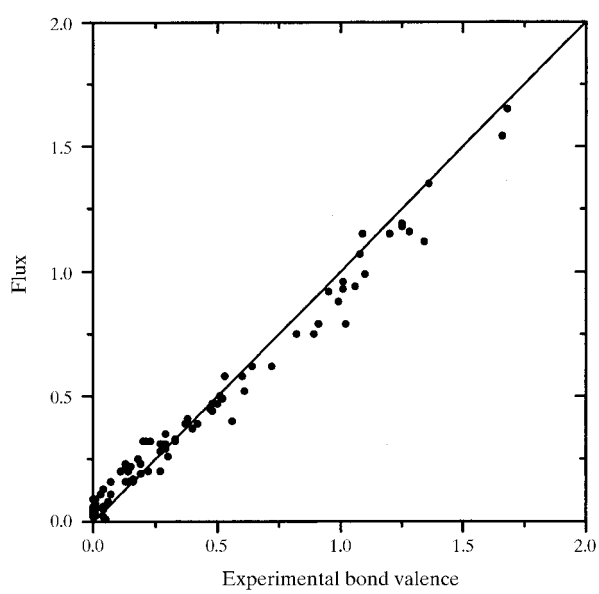

Fig. 9. Flux *versus* experimental bond valences for sterically strained structures.

Fig. 9 compares the flux and experimental bond valence for all sterically strained structures and shows that the agreement between them is almost as good as for unstrained structures. In both cases some of the flux in the stronger bonds has been diverted into the tertiary bonds and for structures with lattice-induced strain there is a little more scatter because the experimental bond valences do not always obey the valence-sum rule. The good agreement between the experimental bond valences and the flux, even in cases where the valence-sum rule is violated, shows that the strain required by the lattice incommensuration is distributed equally between the bonds.

7.3. *Electronically strained structures*

7.3.1. *Lone pair cations*. Electronically induced strains arise from asymmetries in the distribution of electron density around an atom. In these cases $\mathbf{E}_{\mathbf{mult}}$ will make a significant contribution to the local field and the flux determined using $\mathbf{E}_{\mathbf{Madelung}}$ alone is not expected to correspond to the experimental bond valence. If we wished to calculate the true flux linking two atoms it would be necessary to include $\mathbf{E}_{\mathbf{mult}}$, which in turn requires the inclusion of appropriate point multipoles on the atoms. In this study only the Madelung flux has been calculated and it is no surprise that for compounds containing cations with intrinsically anisotropic electron distributions there is poor agreement between Madelung flux and the experimental bond valences (σ_2 in Table 1).

This breakdown can be seen for compounds with stereoactive lone pairs in Fig. 10, which shows the fluxes of the bonds in I_2O_5 plotted against the bond lengths. Also plotted for comparison (broken line) is the correlation between bond valence and bond length given by (14) using the conventional I—O bond-valence parameters, B = 0.37 Å and R_o = 2.003 Å (Brown & Altermatt, 1985). Although the differences are quite dramatic, the fluxes can be fitted to the exponential curve of (14) with B = 0.88 Å and R_o = 1.885 Å (solid line). Similar results are found for the other main group cations in low oxidation state.

For cations with stereoactive lone pairs the electronic anisotropy corresponds to a point dipole oriented with its negative pole directed along the lone pair. Adding this dipole term will decrease the flux of the bonds found on the lone pair side of the cation and correspondingly increase the flux of the bonds on the opposite side, thus strengthening the bonds that are already strong and weakening the bonds that are already weak. It would decrease the value of B from 0.88 Å to a value closer to the Brown & Altermatt (1985) value of 0.37 Å. Unfortunately, there is no easy way to determine the size of the dipole that must be added, hence of calculating the true fluxes in the different bonds.

Alcock (1972) proposed to divide the bonds around lone pair cations into primary and secondary bonds, the primary being typically the three or four strongest bonds and the remainder being secondary bonds. The distinction between primary, secondary and tertiary bonds in these compounds is not as clear as it is for unstrained structures and it is, in general, impossible to classify the bonds in a rigorous way. In particular, there is little virtue in trying to distinguish between secondary and tertiary bonds.

As the electronic strains result in displacements of the atoms, there is no reason to expect that the theoretical bond valences will give accurate predictions for the experimental bond valences. In any case it is not clear if the theoretical bond valences should be calculated using only the primary bonds or using both primary and secondary bonds. For the purposes of comparison, the calculations reported in Tables 1 and 2 have been performed in two ways, in the first case excluding, and in the second case including, the secondary bonds.

7.3.2. *Transition metals*. Many transition metals show electronically strained structures, but the pattern here is different from that shown by the lone pair cations. The anisotropies related to the Jahn–Teller distortions around Cu^{2+} and Mn^{3+} need to be modelled by point quadrupoles on the cation and the anisotropies related to the distortions around the cations with d^0 configurations need to be modelled by point dipoles on the ligands since the distortion involves the polarization of the ligand *p* electrons into the empty *d* shell of the cation (Kunz & Brown, 1995).

Here we focus on the d^0 transition metals, of which V^{5+} is typical. Table 1 shows that the agreement between the fluxes and the experimental bond valences, given by σ_2, while better than for the lone pair cations, is not perfect. The discrepancies can again be examined by plotting the flux against the bond length, as shown in Fig. 11. The points representing the flux lie much closer to the Brown & Altermatt (1985) curve (broken line) than was the case for the lone pair cations, although the fluxes of the strongest bonds are still smaller than the experimental bond valences and the longer bonds have a flux that is significantly larger than the experimental bond valence.

The hypothesis that the fluxes and experimental bond valences are the same cannot be properly tested in compounds with electronically driven strains because of the difficulty of knowing how much the flux will be altered by the inclusion of the multipoles. The calculated Madelung flux for these compounds, while interesting, does not give the full story. There is room for more work to be performed on these compounds.

8. Conclusions

Our calculations show that, apart from the electronically strained structures in which multipole terms are clearly important, the hypothesis that the electrostatic flux and the experimental bond valence are the same is corroborated within experimental uncertainty, the mean value of σ_2 for all structures without electronic strain

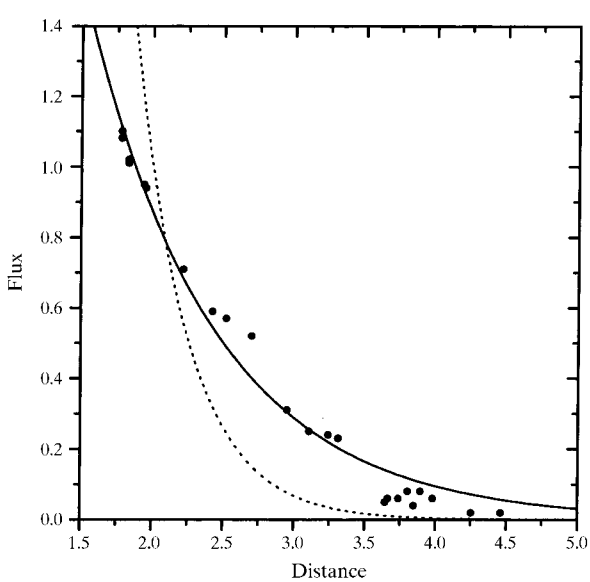

Fig. 10. The Madelung bond flux–bond length correlation for $I^{5+}-O$ bonds. The broken line shows the Brown & Altermatt (1985) parameters. The solid line shows the best fit using R_o = 1.885 Å and B = 0.88 Å (14).

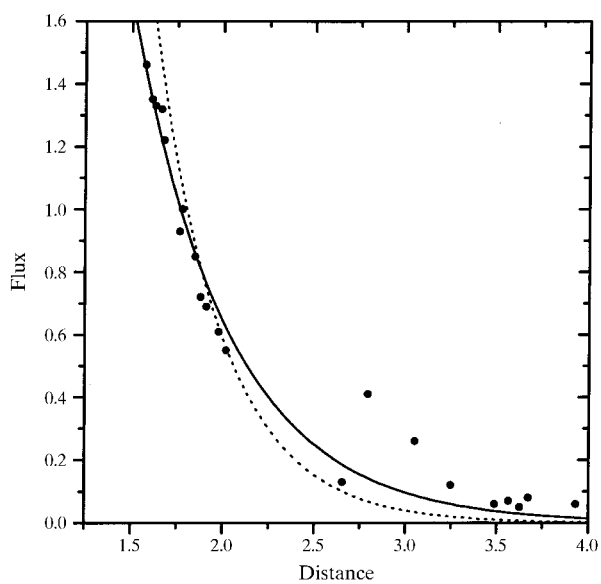

Fig. 11. The Madelung bond flux–bond length correlation for $V^{5+}-O$ bonds. The broken line shows the Brown & Altermatt (1985) parameters. The solid line is the best fit with R_o = 1.768 Å and B = 0.53 Å.

being 0.05 v.u. Even in electronically strained structures there is reason to believe that the hypothesis would be obeyed if the effects of the multipoles could be included.

For unstrained structures the two network equations, which correspond to Gauss' theorem and the law of conservation of energy, give good predictions for the bond valences and fluxes, indicating that at equilibrium the atoms adjust themselves so that all bonds have the same capacitance, C_{ij}. In these compounds $\mathbf{E}_{\mathbf{Madelung}}$ gives a good description of both the short-range and long-range bonding. Even for electronically strained structures the long-range effects continue to be correctly described by $\mathbf{E}_{\mathbf{Madelung}}$. The local field, which includes $\mathbf{E}_{\mathbf{mult}}$, may be responsible for the distortions in the positions of the atoms, but the information about these distortions can only reach distant parts of the crystal through the changes they produce in $\mathbf{E}_{\mathbf{Madelung}}$. Omitting the $\mathbf{E}_{\mathbf{mult}}$ term from our calculations means that they do not correctly describe the local field, but they still give a correct description of the long-range influences that are mediated through Gauss' theorem and hence the valence-sum rule (12).

The results of our study confirm the correctness of the hypothesis that the electrostatic flux linking any two atoms in an inorganic crystal can be identified with the bond valence. This gives a definition for bond valence which requires that the valence-sum rule (12) be exactly obeyed. Failure of the experimental bond valences to obey this rule can be attributed either to a failure of (14) to describe adequately the interatomic repulsion or to geometric constraints in the crystal that prevent the bonds from adopting their chemically ideal lengths. Deviations of the experimental bond valences from their expected values do not therefore indicate a weakness of the model but, on the contrary, provides specific information about the condition of the crystal.

It has been traditional in inorganic compounds to distinguish between ionic bonds, in which electrons are assumed to be transferred from the cations to the anions, and covalent bonds, in which the electrons are shared equally between the atoms. In practice, it is never easy to define the exact degree of ionicity or covalency of a given bond and there is consequently confusion over which is the appropriate model to use. The distinction has been further blurred by the remarkable recent successes of the ionic model in describing structures such as silicates which quite clearly involve covalent bonds (Catlow, 1997). What is frequently overlooked is that the two models are not mutually exclusive in the sense that real bonds are composed of some mixture of ionic and covalent bonding, but that almost all bonds in inorganic solids can be described by either model. A quantitative prediction using the covalent model requires solving the Schrödinger equation for the crystal, but this solution provides a correct description for both ionic and covalent bonds (Bader, 1990). The ionic model is an alternative approach to the same problem which can be applied in any situation in which there is a large Madelung field. It simplifies the calculation by separating the easily calculated classical electrostatic part of the problem from the quantum mechanical part, the latter being treated using the empirically fitted potential $W_{\text{short range}}$. In this paper we have used the ionic model to justify the bond-valence model. Burdett & Hawthorne (1993) have provided a similar justification based on covalent bonding ideas.

The present analysis shows the fallacy of defining ionic and covalent bonding in inorganic materials by the supposed location of the valence electrons in the bond. The distinction that should be made is not where the electrons reside in the bond, but whether the charged atoms have spherically symmetric electron densities. If the atoms carry a charge and are spherically symmetric, $\mathbf{E}_{\mathbf{mono}}$ will be much larger than $\mathbf{E}_{\mathbf{mult}}$ and will dominate the Coulomb field. In this case the ionic or electrostatic model will give a good description of the structure, regardless of where the electrons appear in the bonds. If $\mathbf{E}_{\mathbf{mult}}$ makes a significant contribution as in electronically strained structures, the ionic model has more difficulty predicting the local environments of the atoms, but will continue to describe the long-range effects correctly. Only when $\mathbf{E}_{\mathbf{mono}}$ becomes much smaller than $\mathbf{E}_{\mathbf{mult}}$ will the ionic model fail. This situation will occur when the atoms are far from spherical or when they carry only a small net charge, conditions that are found in metals and many organic compounds. In these cases the ionic model may still be applicable, but it must be used with circumspection.

The distinction between spherical and non-spherical atoms is related to the distinction made by Pearson (1973) between hard and soft atoms. Atoms towards the top and left of the periodic table are hard, that is, they are not easily polarized and remain spherical. Those towards the bottom and right, and in particular some of the transition metals, tend to be soft, that is they are easily polarized and may give rise to large multipole terms in the electrostatic field. Thus, ionic models such as the bond-valence model are expected to work well when the atoms are hard, even for covalent compounds such as silicates, phosphates and sulfates.

By separating the problem of chemical bonding into classical and quantum mechanical components, the classical (Coulomb) part can be easily and rigorously solved, leading naturally to the concept of a localized chemical bond. The quantum mechanical part is short range and treated empirically, but in this paper we show that for equilibrium structures, the solutions that can in principle be found to the Schrödinger equation obey remarkably simple and intuitive rules. Combining the empirical quantum mechanical results with the rigorous classical theory provides insights that can lead to a better understanding of the complexities of chemical bonding.

APPENDIX *A*

In order to determine Φ_{ij} between the atoms i and j, a small equipotential sphere of radius r_s is constructed around atom i. All the lines of field that connect the two atoms will pass through an area A_{ij} on this sphere, and since the field is uniform over the sphere, Φ_{ij} will be proportional to A_{ij}. In order to determine A_{ij} it is only necessary to find its boundaries which can be performed by calculating the paths of a sufficiently large number of lines that pass through the surface.

In order that the equipotential surface can be treated as a sphere it must have a small enough radius. In most cases r_s = 0.01 Å was found to be adequate. The points on the sphere are described in a spherical coordinate system (θ, φ) with $0 \leq \theta \leq \pi$ and $0 \leq \varphi \leq 2\pi$. If n equidistant points are chosen for θ and m equidistant points for φ, the following $(n-1)m$ starting points are obtained: (θ_k,φ_l), where $\theta_k = \pi k/n$, $k = 1,...,n-1$; $\varphi_l = 2\pi l/m$; $l = 0,...,m-1$.

The values of n and m were normally chosen either as (19, 40) or (29, 60). The lines of field are calculated using the gradients of the electrostatic potential U. For a given distribution of point charges q_i at the points $\mathbf{r_i}$ in three-dimensional space, the electrostatic potential U at an arbitrary point $\mathbf{r}$ is defined by

$$U(\mathbf{r}) = \sum_i \{q_i/[4\pi\varepsilon_o(\mathbf{r} - \mathbf{r_i})]\}. \tag{16}$$

The electrostatic field $\mathbf{E}$ is defined by

$$\mathbf{E} = -\text{grad}[U(\mathbf{r})] \tag{17}$$

or

$$E = -[\delta U(x, y, z)/\delta x, \delta U(x, y, z)/\delta y, \delta U(x, y, z)/\delta z]. \tag{18}$$

U($\mathbf{r}$) is calculated using the Ewald method (Ewald, 1921) and the gradient at $\mathbf{r}$ is determined by calculating its three first derivatives. A Cartesian coordinate system is established with its origin at $\mathbf{r}$ and the potentials are calculated at the six points $\mathbf{r} + \boldsymbol{\delta}$ with $\boldsymbol{\delta}$ = (ε,0,0), ($-\varepsilon$,0,0), (0,ε,0), (0,$-\varepsilon$,0,), (0,0,ε,) and (0,0,$-\varepsilon$), ε being a small distance whose size can be varied. In order to calculate the potentials the gradient is assumed to be given by (d_x,d_y,d_z), where

$$\begin{aligned} d_x &= [U(\varepsilon, 0, 0) - U(-\varepsilon, 0, 0)]/2\varepsilon, \\ d_y &= [U(0, \varepsilon, 0) - U(0, -\varepsilon, 0)]/2\varepsilon \\ d_z &= [U(0, 0, \varepsilon) - U(0, 0, -\varepsilon)]/2\varepsilon. \end{aligned} \tag{19}$$

The local coordinates are then transformed to crystal lattice coordinates.

ε was varied during several calculations and a value of 0.001 Å was found to be satisfactory. After the gradient at (θ,φ) on the sphere is calculated, the field line through this point is approximated by a small linear step in the direction of the gradient. The step length can be varied, but a length of 0.01 Å is usually sufficient. Only where the lines are strongly curved was a smaller length necessary. After the first step the gradient at the new point is calculated and the process repeated. After a number of steps (depending on the length of the steps) it was possible to determine to which atom, j, the line would go. The calculation was stopped when the strength of the field exceeded a predetermined value. In this way, for each of the chosen starting points on the sphere the corresponding destination atom was determined. Since the boundary between two bonding regions must lie between two adjacent points that terminate on different atoms, the points ($0.5(\theta_k + \theta_{k+1})$, φ_l) and (θ_k, $0.5(\varphi_l + \varphi_{l+1})$) were taken as an approximation to the boundary. If higher accuracy is needed the boundary region can be examined using a finer grid of starting points. Φ_{ij} is then calculated as

$$\Phi_{ij} = A_{ij}V_i/(4\pi r_s^2). \tag{20}$$

A number of numerical artifacts occurred depending on the choice of the number of terms in the Ewald series for calculating the potentials, the accuracy of the numerical calculation of the derivatives, the radius of the equipotential spheres and the length of the steps along the lines of field. In the neighbourhood of a boundary, field lines were sometimes found that terminated on atoms that were not normally considered to be bonded. Some of these correspond to the tertiary bonds discussed in the text, but some were found to be artifacts of the calculation. In most cases the latter disappeared when the calculation was performed with higher accuracy. Bond regions represented by a single field line were generally ignored.

We wish to thank Richard Bader, Martin Trömel, and Antoni and Hanna Dąbkowski for stimulating discussions. CP wishes to thank the Hermann Willkomm-Stiftung for supporting a flight to Canada which made it possible for him to participate in this research project. JL wishes to thank the European Union for a TMR grant ERBFMBICT 961064, IDB and AS wish to thank the Natural Science and Engineering Research Council of Canada for financial support. MK wishes to thank the Schweizerische Nationalfonds for a research fellowship to spend a year at McMaster University.

References

Alcock, N. W. (1972). *Adv. Inorg. Radiat. Chem.* **15**, 1–57.
Alig, H. & Trömel, M. (1992). *Z. Kristallogr.* **201**, 213–222.
Bader, R. W. F. (1990). *Atoms in Molecules: A Quantum Theory. International Series of Monographs on Chemistry*, Vol. 22. Oxford: Clarendon Press.
Bergerhoff, G., Hundt, R., Sievers, R. & Brown, I. D. (1983). *J. Chem. Inf. Comput. Sci.* **23**, 66–69.
Born, M. & Landé, A. (1918). *Sitzungsber. Pruess. Acad. Wiss. Berlin*, **45**, 1048–1068.
Born, M. & Mayer, J. E. (1932). *Z. Phys.* **75**, 1–18.
Bragg, W. L. (1930). *Z. Kristallogr.* **74**, 237–305.

Brese, N. E. & O'Keeffe, M. (1991). *Acta Cryst.* B**47**, 192–197.
Brown, I. D. (1991). *Chemistry of Electronic Ceramic Materials*, edited by P. C. Davies and R. S. Roth, *NIST* special pub. 804, pp. 471–483. Washington: US Department of Commerce.
Brown, I. D. (1992*a*). *Acta Cryst.* B**48**, 553–572.
Brown, I. D. (1992*b*). *Z. Kristallogr.* **199**, 255–272 (appendix).
Brown, I. D. (1995). *Can. J. Phys.* **73**, 676–682.
Brown, I. D. & Altermatt, D. (1985). *Acta Cryst.* B**41**, 244–247.
Bouhmaida, N., Ghermani, N.-E., Lecompte, C. & Thalai, A. (1997). *Acta Cryst.* A**53**, 556–563.
Burdett, J. K. & Hawthorne, F. C. (1993). *Am. Mineral.* **78**, 884–892.
Catlow, C. R. A. (1997). Editor. *Computer Modelling in Inorganic Crystallography*. San Diego: Academic Press.
Ewald, P. P. (1921). *Ann Phys.* **64**, 253–287.
Gonschorek, W. (1982). *Z. Kristallogr.* **160**, 187–203.
Jumpertz, A. E. (1955). *Z. Electrochem.* **59**, 419–425.
Kisi, E. H. & Elcombe, M. M. (1989). *Acta Cryst.* C**45**, 1867–1870.
Kunz, M. & Brown, I. D. (1995). *J. Solid State Chem.* **115**, 395–406.
Pauling, L. (1929). *J. Am. Chem. Soc.* **51**, 1010–1026.
Pearson, R. G. (1973). *Hard and Soft Acids and Bases*. Stroudsburg, Pennsylvania: Dowden, Hutchinson and Ross, Inc.
Salinas-Sanchez, A., Garcia-Muñoz, J. L., Rodriguez-Carvajal, J., Saez-Puche, R. & Martinez, J. L. (1992). *J. Solid State Chem.* **100**, 201–211.
Shannon, R. D. & Calvo, C. (1973). *Can. J. Chem.* **51**, 265–273.
Stephens, J. S. & Cruickshank, D. W. J. (1970). *Acta Cryst.* B**26**, 222–226.
Wartchow, R. & Berthold, H. J. (1978). *Z. Kristallogr.* **147**, 307–317.
Wu, K. K. & Brown, I. D. (1973). *Mater. Res. Bull.* **8**, 593–598.